Large-Scale Forcing of a Turbulent Channel Flow Through Spanwise Synthetic Jets

Large scale forcing of a turbulent channel flow through spanwise synthetic jets

Journal:	*AIAA Journal*
Manuscript ID	2019-09-J059047.R1
Manuscript Type:	Regular Article
Date Submitted by the Author:	n/a
Complete List of Authors:	Cannata, Marco; Politecnico di Torino, Mechanical and Aerospace Engineering Cafiero, Gioacchino; Politecnico di Torino, Mechanical and Aerospace Engineering Iuso, Gaetano; Politecnico di Torino, Mechanical and Aerospace Engineering
Subject Index Category:	00100 Aerodynamics < 00000 AIRCRAFT TECHNOLOGY, CONVENTIONAL, STOL/VTOL, 01210 Flow Control < 00000 AIRCRAFT TECHNOLOGY, CONVENTIONAL, STOL/VTOL, 20900 Jets, Wakes, and Viscid-Inviscid Flow Interactions < 20000 FLUID DYNAMICS
Select ONE Subject Index for the Table of Contents. This is where your paper will show up in the Table of Contents:	20000 FLUID DYNAMICS

Large scale forcing of a fully developed turbulent channel flow through spanwise directed synthetic jets

M. Cannata*, G. Cafiero † and G. Iuso‡
Politecnico di Torino, Corso Einaudi 40, Torino, Italy

The investigation focuses on the forcing of a fully developed turbulent channel flow through a linear array of synthetic jets injected tangentially to the wall and orthogonal to the mean flow direction. Forcing configurations are varied combining differently the number of actuated jets working in opposition blowing-suction configuration. Instantaneous wall shear stress and streamwise velocity fluctuations evidence drag reductions as well as turbulence attenuation up to 20%. The forcing effects are persistent up to at least 150 half-channel height downstream of the injection section. PIV investigations in planes perpendicular to the channel axis highlight the presence of a large scale streamwise vortical structure covering the whole height of the channel. This structure is thought to be responsible for the significant drag reduction, similarly to the typical behaviour evidenced in the case of colliding jets. The non-dimensional forcing frequency of the synthetic jets producing the maximum drag reduction and turbulence attenuation is 0.0074 for the investigated Reynolds number (Re_τ=180). A statistical analysis of the near wall structures demonstrates that the control mechanism acts in a way to reduce them in the forced configuration. We conclude that the effect of the forcing is such that the near wall structures merge and become less prone to induce new structures, thus effectively reducing their number and consequently the near wall turbulence activity.

I. Nomenclature

B	=	channel breadth
c_P	=	$(p - p_{ref})/(0.5\rho U_c^2)$ pressure coefficient
E	=	power spectrum
f	=	sampling frequency
f_f	=	forcing frequency
H	=	channel semi-height
L_{char}	=	characteristic forcing length

*Engineer, Department of Mechanical and Aerospace Engineering
†Assistant Professor, Department of Mechanical and Aerospace Engineering, Corso Einaudi 40 Torino
‡Full Professor, Department of Mechanical and Aerospace Engineering

L_0/d	=	dimensionless stroke length
L_x	=	longitudinal characteristic length of near wall structures
L_z	=	transverse characteristic length of near wall structures
p	=	static pressure
$R_{u'u'}$	=	autocorrelation function
Re	=	$U_c H/\nu$ Reynolds number
Re_τ	=	$u_\tau H/\nu$ friction Reynolds number
Sr	=	fH/U_c Strouhal number
U_c	=	centerline velocity in the unforced configuration
U_j	=	characteristic jet velocity
u_τ	=	friction velocity
$\overline{V}$	=	velocity vector
W	=	spanwise velocity component
X	=	streamwise coordinate
Y	=	wall normal coordinate
Z	=	spanwise coordinate
δ_v	=	ν/u_τ viscous unit
λ_s	=	streaks' spacing
ρ	=	air density
ν	=	air kinematic viscosity
τ_w	=	wall shear stress
SUPERSCRIPTS	=	
f	=	forced configuration
+	=	inner variables normalization
ACRONYMS	=	
DNS	=	direct numerical simulation
PIV	=	particle image velocimetry

II. Introduction

WALL turbulence control has represented one of the driving forces for fluid dynamic research over the past decades. The possibility of reducing skin friction drag, particularly attractive in the aeronautical field, pushed both fundamental as well as industrial research. Many flow control strategies have been proposed ranging from passive

techniques to very complex active systems that also include a sensors-actuators feedback operation. While the former approach is generally reliable but unavoidably affected by the problem that it works properly for one only design condition, the latter is very often too complex to be implemented in realistic applications, such as an aircraft wing.

Within this last group surely falls the transverse forcing applied to the mean flow. Several studies demonstrated the effectiveness of such control strategy, leading to significant reduction of the skin friction coefficient as well as attenuating the turbulence fluctuations. Jung et al. [1] performed DNS calculations of a fully developed turbulent channel flow forced by a spanwise oscillating wall. They observed that the percentage of drag reduction was dependent on the wall oscillation period. At proper values of this last parameter (T^+=100, whereby the superscript + indicates the normalization according to inner variables), the mean skin friction was reduced by 40% and the streamwise Reynolds stress component exhibited a similar behaviour. The authors also showed that the same results can be obtained if transverse oscillations are imposed to the mean flow. Choi et al. [2, 3] showed similar drag reductions using the same technique, with a 45% reduction in the wall shear stress. Straub et al.[4] applied spanwise oscillation to a turbulent duct flow having aspect ratio equal to 3, showing similar values of drag reduction. Baron and Quadrio [5] looked at the total energy budget by means of DNS calculations performed on a 2D channel flow forced by spanwise periodic wall oscillations. At T^+=100 and for spanwise wall-oscillation amplitudes equal to $Q_x/8h$ (Q_x is the streamwise flow rate per unit width and h is the channel half height), they reported a 10% net energy saving. More recently, Gatti and Quadrio [6] investigated the effect of the Reynolds number on the effectiveness of such control mechanism. They concluded that, for sufficiently large Reynolds number values, a constant 30% value of drag reduction can be obtained. Furthermore, they detailed that, similarly to other wall-based drag reduction techniques, the performance of the spanwise oscillation is well described by an upward shift of the logarithmic portion of the mean streamwise velocity profile.

Di Cicca et al.[7] performed measurements by means of PIV techniques in a turbulent boundary layer developing on a flat plate under the effect of spanwise wall oscillations characterized by T^+=100 and by an oscillation amplitude of Δz^+=320. The authors highlighted a reduction in the mean velocity gradient near the wall and, at the same time, they also reported reductions of the streamwise (30%) and wall normal (40%) turbulent velocity fluctuations. Moreover, the turbulent kinetic energy production was minimized by 35%.

The extremely promising values of drag reduction obtained via spanwise oscillations are at odds with the actual implementation of such technique. In this light, numerous efforts have been spent with the aim of reproducing similar near wall configurations of the flow field without the need of having a moving wall.

Effective drag reductions in wall bounded flows can be obtained using large scale forcing. Numerous investigations dealt with such control mechanism. Schoppa and Hussain [8] performed direct numerical simulation and showed the effectiveness of large scale forcing in a turbulent channel flow. They found 20% drag reduction in the case of counter-rotating streamwise vortices and 50% drag reduction for the colliding spanwise wall jets. Iuso et al. [9] experimentally investigated the effects of the injection of convergent couples of continuous jets in a channel flow. They

showed the effectiveness of such control mechanism over long distances from the injection section both in terms of drag reduction (30%) and turbulence attenuation (50%). Similar results were obtained by Di Cicca et al. [10] forcing a turbulent boundary layer by means of counter-rotating large scale streamwise vortices. Also direct numerical simulations (DNS) from Yao et al.[11, 12] recently confirmed that drag reductions could be obtained with large scale near-wall opposite wall-jet control in the range of Re_τ=80 to 550 delivering drag reduction from 19% to 12% respectively. The choice of the authors of defining the control mechanism as large scale even though it scales in inner units is justified by the relatively low value of the Reynolds number.

Canton et al. [13, 14] performed the control of a low Reynolds number fully developed turbulent channel flow using a large-scale flow control strategy considering the control scheme of Schoppa and Hussain [8]. The authors showed that at Re_τ = 180 a maximum drag reduction is reached employing vortices with a wavelength $\lambda^+ = \lambda/\delta_v$= 1200; with this configuration, they obtained a drag reduction of 18% ($\delta_v = u_\tau/\nu$ indicates the viscous height). The authors also made the point that effect of such control mechanism on higher Reynolds number flows and the appropriateness of the definition of large scale forcing would require dedicated investigations. In particular, regarding the first point, it is indeed expected a lower effectiveness of the control system at higher Reynolds numbers (also demonstrated by [12].

Jukes et al.[15] reproduced a spanwise oscillating flow by using plasma actuators that led to drag reductions as large as 45%. The effect of the plasma was such that introduces a tangential force near the wall, which in turns generates co-rotating streamwise vortices in the inner region of the boundary layer. Du et al. [16] proposed the use of spanwise travelling waves to force wall-bounded flows in order to achieve turbulent skin friction drag reduction. Karniadakis and Choi [17] carried out an extensive review of the topic, with particular emphasis on the mechanism related to transversal motions in wall bounded flows considering both passive and active strategies.

The periodic flow field generated by synthetic jets [18–20] has been proposed as a possibility to reproduce the effects of a moving wall. This kind of forcing has been successfully applied for flow control as it enables the possibility to generate different time-space forcing scales, according to the characteristics of the flow. Given their versatility, synthetic jets have been applied to countless applications, including wings virtual shaping [21], heat transfer enhancement [22] and thrust vectoring [23].

Within the flow control scenario, Park et al.[24] manipulated the turbulent boundary layer developing on a flat plate by injecting a synthetic jet through a spanwise slot and showed that the forcing produced a drag reduction. Iuso and Di Cicca [25] and Iuso et al. [26] forced a fully developed turbulent channel flow by means of couples of non-parallel synthetic jets; their effect resulted in the production of large scale streamwise vortices which reduced the skin friction and the turbulent fluctuations near the wall.

Finally, several attempts have been proposed to passively induce spanwise flow oscillations. In particular, the use of micro roughness opportunely shaped to induce a wavy motion in addition to the streamwise one was experimentally and numerically exploited [27–31].

The present investigation focuses on a fully developed turbulent channel flow that is transversally forced by the imposition of periodic oscillations through a linear array of ten synthetic jets. The injection orifices are flush-mounted on a vertical wall of the channel and aligned to the streamwise direction. They are split into two blocks working in opposition (blowing-suction configuration). The number of synthetic jets connected to each block is variable, thus allowing for different forcing configurations. The effects of the actuation frequency as well as of the injection configurations on the drag and on the turbulence structure of the channel are analysed and discussed in terms of local (wall shear stress) and global (Particle Image Velocimetry) measurements.

III. Experimental setup and measurements techniques

The experiments are performed in a rectangular cross-section channel flow at Politecnico di Torino. The channel is characterized by a half channel height (H) and breadth (B) respectively equal to 10mm and 280mm; the channel length is 8m. A 2m portion of the channel located 133 hydraulic diameters (5m) downstream of the inlet section, constitutes the test section where the measurements are carried out (see Figure 1). A complete description of the channel is reported by Iuso et al. [25]. The reference frame is defined in a way such that the origin for the streamwise coordinate X corresponds to the location of the last jet injection (see Figure 1b), while Z indicates the spanwise coordinate. The wall normal direction is indicated with Y and originates at the top wall of the channel. The experiments were carried out at a fixed Reynolds number $Re = U_c H/\nu \approx 3{,}600$, where U_c is the centreline velocity in the unforced configuration (equal to about 5.4m/s for this set of experiments). This corresponds to a Re_τ=180, based on the friction velocity (u_τ) and the half-channel height H.

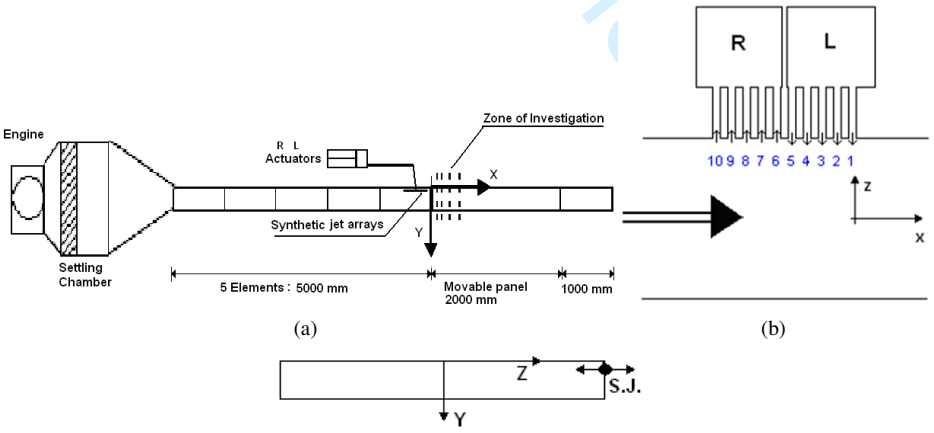

Fig. 1 Schematic representation of the channel flow and indication of the reference frame: a) side view with indications of the investigated planes, either by pointwise or PIV measurements; b) top view with schematic representation of the jet injection and c) rear view, i.e. looking from the channel exit section. Drawing not to scale.

The injection orifices for the synthetic jet forcing are located on one of the two lateral walls; the injection occurs

in the XZ plane transversally to the mean flow direction through 10 tubes (internal dimeter d equal to 2mm) located upstream of the test section in the range of streamwise distances -2.9< X/H <0 and at a constant height $Y/2H$ =0.0625 (Fig. 1b). The ten injection orifices are equally spaced in the streamwise direction, with a centre to centre distance equal to 1.5d (3mm).

The synthetic jet actuator is obtained from the oscillating system of a commercial airplane model engine. The piston diameter and stroke are respectively equal to 30.4mm and 27.5mm. Two different actuators are employed, indicated as R and L in Fig. 1b; each actuator fed different groups of orifices. The actuators operated in opposition phase to modulate the forcing in the streamwise direction: the piston of one actuator at the extreme lower stroke end is located opposite to the piston of the other. Therefore, when one actuator is in blowing phase, the other is in suction phase and vice-versa. Both actuators are connected through two cogged wheels to a brushless electric motor whose angular speed allowed the variation of the forcing frequency, while the amplitude is kept constant.

A Plexiglass interface cylinder with the same internal diameter of the piston and closed on its top is mounted on the top part of each piston. Ten holes located on the top of the cylinder are connected to the injection points on the channel wall. The height of the cylindrical plexiglass cavity is equal to 50mm. The estimated resonance frequency of the cavity is in the range 230-260Hz, depending on the extreme positions assumed by the piston during a cycle.

Simultaneous measurements of wall shear stress and velocity fluctuations are performed and conditioned to the position of the pistons. To this end, on the shaft of actuator L a pick-up magnetic sensor gives in output a voltage signal in the range 0-5 V depending on the piston position. The maximum voltage pertained to the uppermost location of the piston L, hence corresponding to the lowest location for the piston R.

Different injection configurations of the synthetic jets were considered to investigate the different effects on the flow field organization. Instantaneous wall shear stress and streamwise velocity measurements are performed by means of hot wire probes. The former is manufactured in-house and constituted by a cylindrical plexiglass base flush mounted to the wall. The hot–wire sensor is soldered to two metallic prongs fixed into the base, allowing the sensor to lie in the middle of the flush mounted face over a small cylindrical cavity. A detailed description and validation of the wall shear stress probe is given by Spazzini et al [32]. The presence of the cavity improves the probe sensitivity by reducing the heat losses towards the plexiglass substrate as reported by Tardu and Pham [33].

The length of the wire is approximately 1.2mm, whilst the wire diameter was 5μm, thus resulting in a the length of the wire scaled in inner units of about 21, which is slightly above the recommended value by Shah and Antonia [34] and Hutchins et al.[35]. Nevertheless, this does not represent any concern for the present case where the natural flow is compared to manipulated cases with the same flow conditions and probe. The only shortcoming might be related to slightly attenuated values of wall shear stress RMS values.

The wall shear stress sensor is calibrated in situ before each test. The output signal from the wall shear stress probe was directly related to the measured pressure gradient which accounts for the wall shear stress value. The calibration

was performed varying the channel flow conditions from laminar to turbulent flow regime.

A boundary layer hot wire probe is employed for the streamwise velocity measurements. The probes' calibration is performed in-situ correlating the output voltage to the pressure gradient measured along the channel. Both the wall shear stress and hot wire probe were powered by a AN-1003 anemometer system. Both signals were sampled after a low pass filter set to 6kHz, using a National Instruments data acquisition board (PCI-MIO-16-XE-10) with a 16 bits A/D converter. Data were acquired for 180s at an acquisition frequency set to 12kHz, thus ensuring the proper convergence of the statistics.

The ratio between the rms value of the wall shear stress fluctuations and the mean value $\tau_{w,RMS}/\tau_w$ is equal to 0.30 while the flatness and the skewness are respectively 4.2 and 0.98. These values are in good agreement with the those reported by Wietrzak and Lueptow [36].

Both the hot wire and the wall shear stress measurements were repeated many times, to verify repeatability of the results. All the tests showed repeatable results within ±2% of the reported value.

Static pressure distributions are measured along the channel centreline and at different spanwise positions using a Scanivalve system and a Setra pressure transducer. In the light of minimizing the number of pressure taps distributed along the channel walls, the spanwise measurements are performed by transversally displacing the upper wall of the channel. In order to comply with this constraint, the upper wall is designed with a breadth significantly larger than B.

Particle image velocimetry measurements are carried out in the YZ plane at two streamwise locations, corresponding to those where the control mechanism was found to be the most effective, namely at X=38H and X=48H. The size of the imaged area was 100x70mm, resulting in a digital resolution equal to 13pixel/mm. Moreover, PIV measurements are also performed in the XZ plane at a wall distance equal to y^+=12. In this case the imaged area was 28x24mm, resulting in a digital resolution of 45pixel/mm. For each case, one thousand statistically uncorrelated snapshot are acquired using a 1Mpixel PCO Sensicam (1280x1024 pixels resolution) equipped with a 100mm Nikon lens. The acquisition frequency was set to 10Hz and the time delay was set to 60 μs. The channel flow is seeded using a commercial smoke generator; the injection occurred upstream of the centrifugal blower, to ensure a sufficiently homogeneous distribution of the tracing particles. The cross-correlation is performed using the commercial software developed by Dantec Dynamics which is based on a multi-step approach, with a final interrogation window size equal to 32x32 pixels (about 0.7x0.7mm) and 50% overlap, thus resulting in a vector pitch equal to 0.35mm.

IV. Effect of the forcing configuration

A preliminary characterization of the forcing system was performed directly in the channel without base flow. The effects of the forcing related to the different array configurations and to the forcing frequency are presented in this section.

A. Synthetic jets characterization in still air

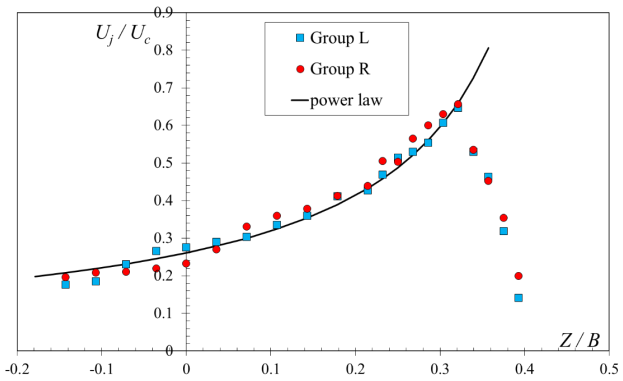

Fig. 2 Velocity distribution along the spanwise direction (i.e. the jets' axial direction) in absence of mean flow. The synthetic jets are operated at $f_f H/U_c$=0.0074. The array configuration is (L_{1-5} R_{6-10}).

This basic characterization was performed in terms of velocity distributions of the synthetic jets in the centre of each group (L and R) forming a specific forcing array (L_{ij}-R_{ij}, being i the first and j the last actuated jet of that particular array). The objective of this analysis is twofold: the evaluation of the representative velocity of the forcing array along the spanwise direction of the channel (Z/B) and the estimate of the penetration length of the synthetic jets along the spanwise direction of the channel. For the sake of conciseness, we report the results corresponding to only one array configuration that we consider as the most representative for the present study, namely L_{1-5}-R_{6-10}, for which the forcing frequency f_f equals to 4Hz (corresponding $f_f H/U_c$=0.0074). As it will be shown later in the paper, this forcing condition corresponds to the most effective in terms of skin friction reduction.

Fig. 2 reports the non-dimensional jet velocity U_j/U_c profile as a function of the spanwise distance, where U_c indicates the centerline velocity in the channel in the uncontrolled case (i.e. natural case). The distribution shows increasing values of the velocity along Z/B from the wall injection side up to $Z/B \approx$0.32 where the velocity of both groups of jets reaches the maximum value of U_j/U_c=0.65. Proceeding towards the centre of the channel, the velocity decreases in accordance with the typical power law decay of isolated continuous and synthetic jets: $k(Z/B)^{-m}$. The value of the exponent m is slightly different from that of the isolated synthetic jets, as the confinement introduced by the upper wall of the channel as well as the effect of multiple jets at close distance was demonstrated to influence the streamwise evolution of the flow [37]. The fitting coefficients k and m in the decay law are equal to 0.14 and 0.90, respectively. As shown in Fig. 2, the velocity field of the jets is consistently persistent even beyond the channel axis (Z/B=0).

B. Effect of synthetic jets' configuration and actuation frequency

Wall shear stress measurements of different synthetic jets array configurations and various forcing frequencies are carried out for different streamwise and spanwise positions.

Configuration	L_1 R_10	L_{1-2} R_{9-10}	L_{1-3} R_{8-10}	L_{1-4} R_{7-10}	L_{1-5} R_{6-10}
$U_{j,max}/U_c$	0.24	0.33	0.49	0.58	0.65

Table 1 Tested configurations and corresponding maximum velocity amplitudes of the synthetic jet compared to the channel centreline velocity.

Tab. 1 summarizes the tested configurations and the corresponding forcing amplitudes, quantified as the ratio between the maximum jet velocity along its axis in still air conditions and the centreline velocity of the channel in the natural case. Five synthetic jet configurations are tested by connecting an increasing number of orifices to each

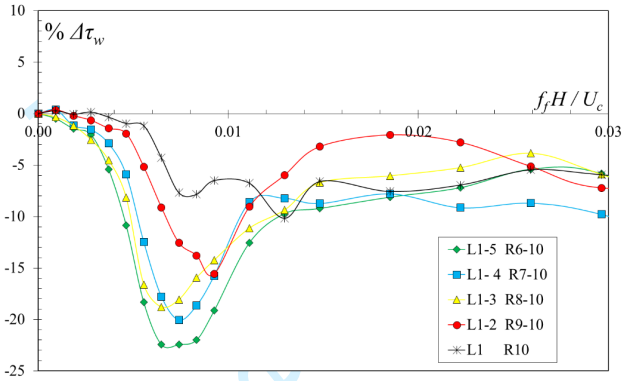

Fig. 3 Percentage variations of the mean wall shear stress τ_w as a function of the non-dimensional forcing frequency $f_f H/U_c$. Data are measured at X=38H and Z=0.36B.

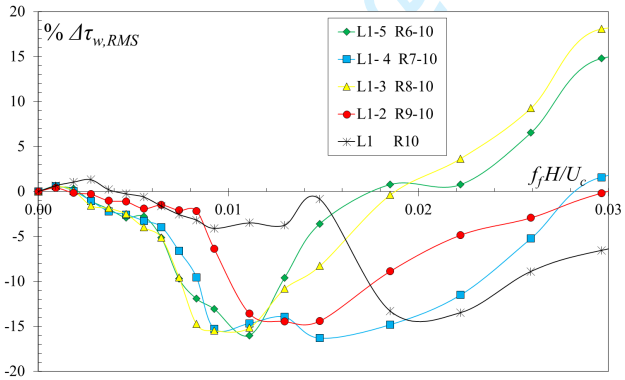

Fig. 4 Percentage variations of the rms wall shear stress $\tau_{w,RMS}$ as a function of the non-dimensional forcing frequency $f_f H/U_c$. Data are measured at X=38H and Z=0.36B.

actuator, as reported in Tab. 1. Fig. 3-4 show the percentage variations in the mean wall shear stress (τ_w) and its root mean square ($\tau_{w,RMS}$) measured in correspondence of the top wall at X=38H and Z=0.36B, as a function of the non-dimensional forcing frequency $f_f H/U_c$.

All forcing configurations exhibit drag reductions for a wide range of frequencies ($0.004<f_f H/U_c<0.02$). A more detailed inspection of Fig. 3 suggests that the control configuration leading to the minimum wall shear stress entails

the simultaneous activation of the ten synthetic jets, namely L_{1-5} R_{6-10}. The maximum effectiveness of the control mechanism is achieved for a non-dimensional actuation frequency $f_f H/Uc \approx 0.008$. Nevertheless, increasing the number of connections shows a detrimental effect for higher values of the actuation frequency.

Fig. 3 shows that for $f_f H/U_c > 0.014$ the maximum effectiveness is obtained for L_{1-4} R_{7-10}. Furthermore, irrespective of the actuation frequency values, the wall shear stress reduction locks in to a nearly constant value, which differs for every control configuration. The highest drag reduction was obtained in the configuration L_{1-5} R_{6-10}, featuring a wall shear stress reduction of 22.4% at $f_f H/U_c$=0.0074. It is also interesting to notice that, as evidenced in Fig. 4, in a similar range of actuation frequencies a significant reduction of the wall shear stress fluctuations can also be detected, regardless the actuation mechanism. The only one exception is the L_1 R_{10} actuation configuration, which proves to be ineffective for the presented flow conditions.

In the light of the results of Fig. 3 and Fig. 4, we identify the best forcing configuration with L_{1-5} R_{6-10}, as it features the highest values of mean and fluctuating wall shear stress reductions. In particular, for the forcing frequency $f_f H/U_c$ =0.0074 drag reductions as large as 22.4% can be obtained with a corresponding 10% turbulence attenuation.

V. Flow field structure: velocity, wall shear stress and pressure analysis

We hereby report the spatial organization obtained for the reference forcing configuration (L_{1-5} R_{6-10}, $f_f H/U_c$ =0.0074). Fig. 5 shows the time-averaged velocity vector fields measured in the YZ plane at two streamwise locations, namely X=38H and X=48H. The jet injection is located at a distance $Y/2H$=0.0625 from the horizontal upper wall, at Z/B=0.5.

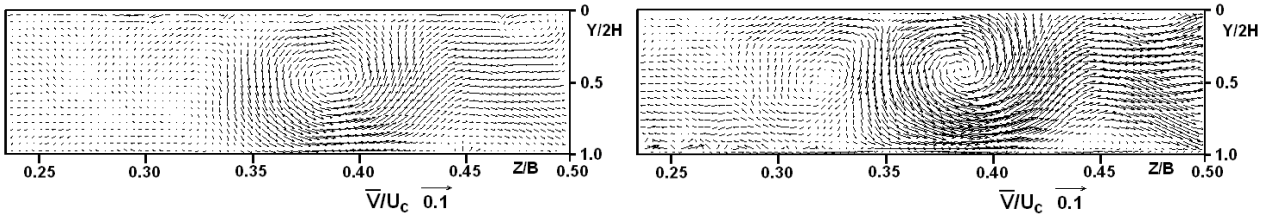

Fig. 5 Time averaged velocity field in the YZ plane at (a) X/H=38 and (b) X/H=48 (rear view).

The mean velocity fields highlight the presence of a large scale counter-clockwise vortical structure whose centre is positioned at $Z/B \approx 0.38$ for both streamwise locations. The vortical structure covers the whole channel height and more than the channel height in the spanwise direction. Also, intense shear layers are present on the right side of the vortex, in the region between the main vortex and a first secondary structure located near the bottom wall of the channel at $Z/B \approx 0.45$. More interestingly, the main structure induces a secondary large scale structure that becomes more evident at larger streamwise distances (X/H=48). Berk and Ganapathisubramani [38] recently showed that a synthetic jet in

cross-flow configuration produces couples of counter rotating vortices. These structures are ascribed to the distortion of the vortices produced by the synthetic jet itself. In the present case, where more than one synthetic jet alternatively lows in cross-flow, a packet of such structures in created and stays limited within the boundaries imposed by the channel walls.

This flow configuration closely resembles the one reproduced in the case of colliding jets, as described by Schoppa and Hussain [8] and Yao et al [12]. In their recent paper, Yao et al [12] pointed out in their numerical simulation of colliding jets the performance of such control mechanism in terms of drag reduction were worth of merit. The self-induction of a counter-rotating large scale vortex induced by the main structure may provide a leap forward in the actual implementation of such technique.

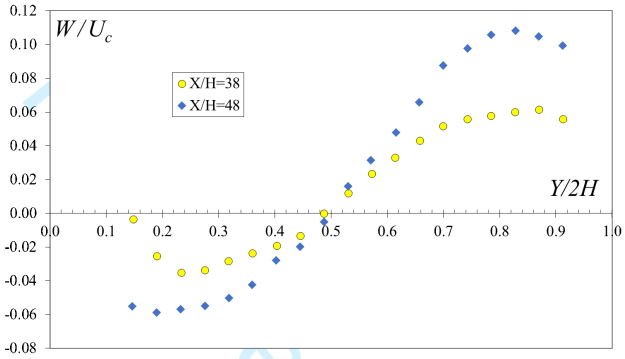

Fig. 6 Transversal mean velocity measured in correspondence of the vortex core location in the spanwise direction (Z/B=0.38) at X/H=38 and X/H=48.

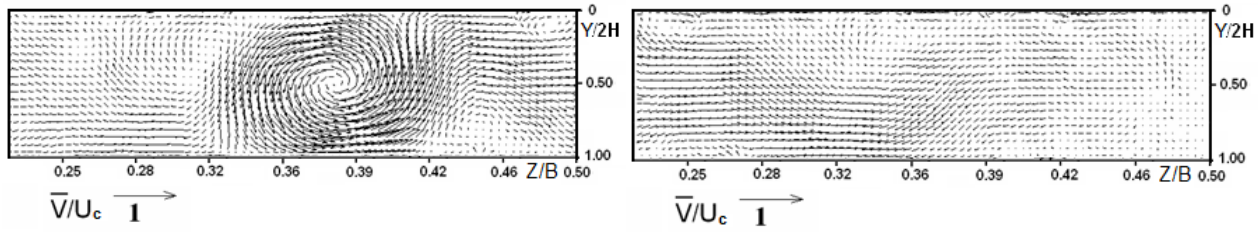

Fig. 7 Averaged flow field conditioned to the presence (a) and the absence (b) of the vortex in the YZ plane. Data are measured at X/H=38. (rear view).

Fig. 5a-b suggest that the vortical structure is more intense at X=48H with respect to X=38H. The intensification of the vortex at higher streamwise locations is also evident from the results reported in Fig. 6, showing the non-dimensional mean velocity distributions of the spanwise velocity component W/U_c along the wall normal coordinate. The profiles are extracted in correspondence of the vortex cores (Z/B=0.38). At larger streamwise distance, a significantly stronger shear rate can be detected from the results of Fig. 6. Further to this, the wall normal extent of the linear velocity distribution that identifies the vortex core is larger at X=48H with respect to X=38H, thus suggesting an increase in size

of the structure covering the whole channel height.

Given the nature of the forcing mechanism, the vortex is expected to be present only intermittently. An attempt to identify only those instances where the main vortical structure is present is based on the technique proposed by Scarano et al. [39]. The cross-correlation of the instantaneous velocity field with a Lamb–Oseen vortex pattern was evaluated and the local maxima was considered as the vortex centre if this function exceeds an arbitrarily chosen threshold level. From this analysis resulted that 35% of the vector fields were characterized by the presence of the main vortex.

The averaged flow fields conditioned to the presence or the absence of the main vortex are reported in Fig. 7. As expected, the flow field conditioned to the presence of the vortex (Fig. 7a) closely resembles the time averaged flow field showed in Fig. 5, whereas the one obtained by averaging the flow fields where the vortex is absent is characterized by shear layers of different extent and intensity and by small scale motions.

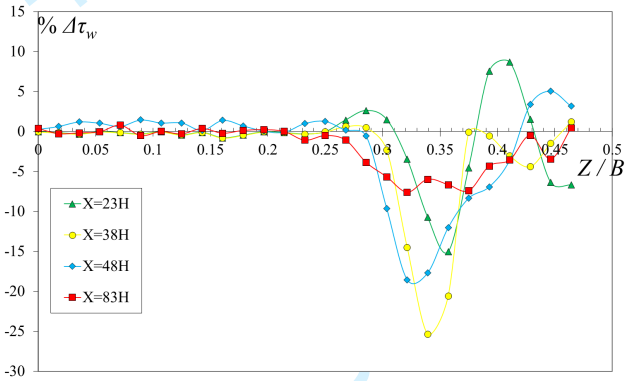

Fig. 8 Percentage variations of the rms wall shear stress τ_w in the forced configuration (L_{1-5} R_{6-10} at $f_f H/U_c$=0.0074) as a function of the spanwise coordinate Z/B. Data are measured at X/H=23, 38, 48 and 83.

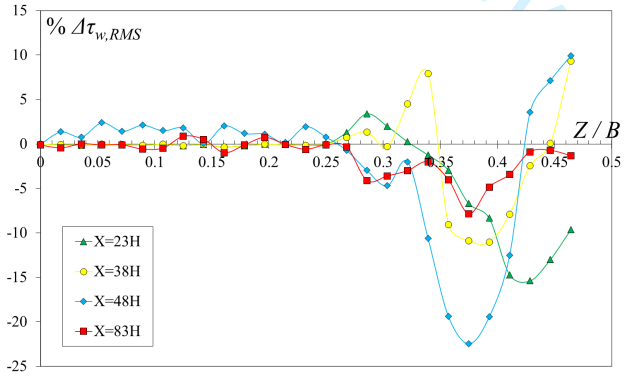

Fig. 9 Percentage variations of the rms wall shear stress $\tau_{w,RMS}$ in the forced configuration (L_{1-5} R_{6-10} at $f_f H/U_c$=0.0074) as a function of the spanwise coordinate Z/B. Data are measured at X/H=23, 38, 48 and 83.

In Fig. 8-Fig. 9, the spanwise percentage variations of the mean and rms wall shear stress are shown as a function of the spanwise coordinate Z/B. Data are measured at $Y/2H$=0 and in the range of streamwise distances 23< X/H <83

and for the reference forcing configuration ($L_1 - 5\ R_6 - 10$ at $f_f H/U_c$=0.0074).

The effect of forcing, for all the streamwise locations, persists along the spanwise direction up to $Z/B \approx 0.22$. Additionally, for each streamwise location, a well-defined spanwise range of the channel is characterized by both drag reduction and wall turbulence attenuation. In particular, even at distances as large as $83H$ from the injection region, the wall shear stress reduction is still significant (nearly 7.5%). As evidenced by the velocity fields results showed in Fig. 5, the largest local reduction of the mean wall shear stress occurs where the vortex induces upwash from the top wall. Similar results were obtained by Yao et al [11]. They showed that the optimal height of the colliding jets was about $y^+ \approx 30$, which is reasonably close to the one that is reproduced in the current case ($y^+ \approx 23$).

Correspondingly, an increase of the wall shear stress can be detected where the fluid is pushed towards the top wall. Nevertheless, the latter effect is less intense than the former, (particularly from $X/H > 38$), thus producing an overall beneficial effect of the control mechanism. We address this difference to the interplay between the impinging fluid and the one induced by the forcing mechanism. Similar observations were drawn by Iuso and Di Cicca [25], Di Cicca et al. [7] and Iuso et al. [9], with different forcing configurations. They showed that the presence of large scale longitudinal vortices in a wall bounded flow gives rise to three typical regions. Namely, these regions correspond to the up-flow, down flow and cross-flow regions induced by the large scale vortex. All these three regions have a beneficial effect regarding the attenuation of the near wall turbulence activity, resulting in a reduction of the fluctuating wall shear stress, as reported in Fig. 9 for the present investigation.

From a phenomenological standpoint, the structure induced by the large scale vortex acts in a way similar to the case of colliding wall jets, reproducing similar values of drag reductions. The effect of the colliding jets is indeed such that they cause the merger of multiple streaks together into a larger streak envelope so that its strength drops below critical values for transient growth. For $X/H > 83$ the effects of the forcing are attenuated, and the flow tends to recover the uncontrolled conditions.

The same investigation was performed on the opposite horizontal wall. The results were similar to those reported in Fig. 8-Fig. 9.

We evaluated the global effect of forcing on the channel top and bottom wall, in order to give a direct grasp of the drag reduction that can be achieved using such control mechanism. For each streamwise position, the percentage variations reported in Fig. 8-Fig. 9 are integrated over the spanwise direction. In Fig. 10, the percentage variations of the integrated spanwise wall shear stress and of its fluctuation distributions are plotted as a function of streamwise distance X/H. It can be observed that, beyond X/H=22, both channel walls are characterized by drag reduction and wall turbulence attenuation up to streamwise distances as large as X=153H from the forcing section. While the mean wall shear stress is characterized by a similar behaviour on both channel walls, the rms features a significantly different trend. In particular, the wall opposite to the injection side (Y=2H) features much stronger reductions. As evidenced in Fig. 5, the main vortex triggers the presence of a smaller secondary structure near the wall opposite to the one

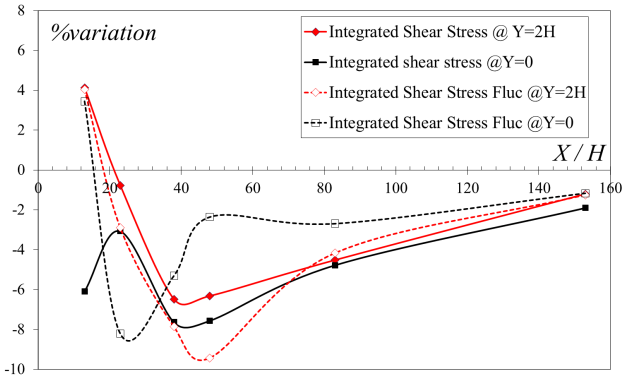

Fig. 10 Spanwise integrated drag reduction and turbulence attenuation along the streamwise direction. Forcing configuration $\mathbf{L}_{1-5}$ $\mathbf{R}_{6-10}$ at $f_f H/U_c$=0.0074.

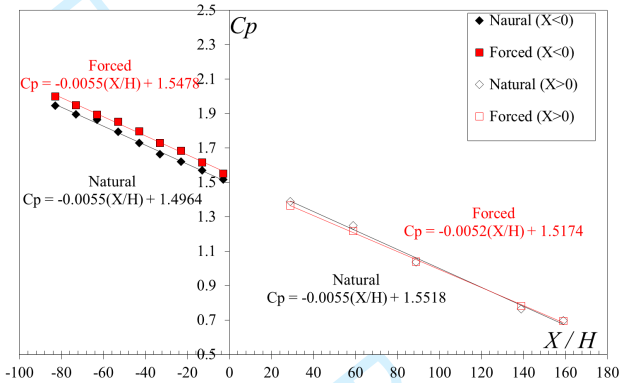

Fig. 11 Streamwise pressure distributions along the channel upstream and downstream of the forcing section.

of injection. This vortex could be responsible for the further reduction in the wall shear stress fluctuations. Beyond X/H=120 this effect is dissipated.

Fig. 11 reports the pressure coefficient ($c_p = (p - p_{ref})/(0.5\rho U_c^2)$) distributions along the channel measured at Z/B=0.36, for the natural and forced case. The best fit lines and the percentage variations in the pressure gradients are also displayed in the same plots. The pressure distributions are measured upstream and downstream of the forcing arrays and only on the top wall ($Y/2H$=0). Upstream of the injection, no significant variation in the pressure gradient can be detected, besides a slight upward shift of the curve which could be related to the effect of blockage imposed by the blowing jets; more interestingly, for X/H>0 the streamwise pressure gradient reduces with respect to the natural case, as the pressure gradient reduces of about 5.4%.

The streamwise mean and rms velocity profiles are plotted in Fig. 12-Fig. 13. Data are measured at a fixed spanwise location (Z/B=0.36) and at different streamwise positions (X=13H, X=23H,X=38H and X=83H). Measurements were performed starting from the top wall ($Y/2H$=0). At X=23H, the investigation was also extended to the opposite wall. As a reference, the velocity profile of the natural case is also reported. All data are normalized with respect to inner variables, i.e. with respect to u_τ and δ_v calculated in the natural case.

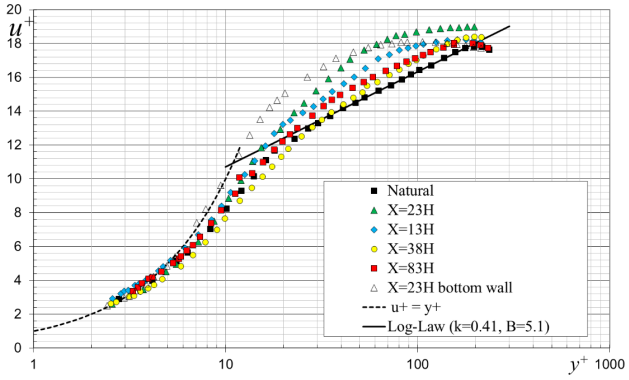

Fig. 12 Mean streamwise velocity as a function of the wall normal distance measured at X/H=13, 23, 38, 83. Measurements are performed on the top wall; at X/H=23, the measurements are also extended to the wall opposite to the injection side.

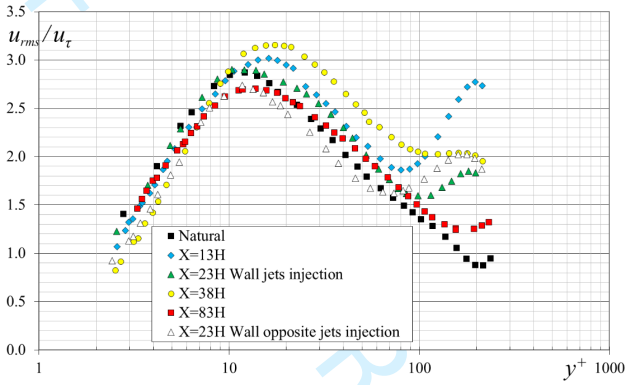

Fig. 13 RMS of the streamwise velocity as a function of the wall normal distance measured at X/H=13, 23, 38, 83. Measurements are performed on the top wall; at X/H=23, the measurements are also extended to the lower wall.

The control mechanism shows a strong effect on the mean velocity profiles, particularly for y^+ >7. Indeed, the well-defined log-layer evidenced in the natural case is strongly perturbed by the forcing. A significant enhancement of the streamwise velocity values is detected in the range of streamwise distances 13<X/H<23. At larger streamwise distances, this effect eventually fades out. Furthermore, it is particularly interesting to notice that, the velocity profile measured on the wall opposite to the jet injection (open symbols) does not show a clear log-layer. This result seems to suggest that on this side of the channel the mean velocity profile approaches the pure viscous regime (also reported as a reference in the plot), rather than the turbulent one.

Fig. 13 evidences that only in the region near the wall the turbulent fluctuations reduce in comparison to the natural case, accordingly with the attenuations of the wall shear stress fluctuations. For increasing wall normal distances, an opposite effect is visible. In the forced case, the peaks of the velocity fluctuations are mainly shifted towards larger distances from the wall as the streamwise distance X/H increases up to X/H=38. For X/H=83, as in the case of the mean velocity profiles, the distribution of u^+_{RMS} approaches the natural case. A similar behaviour of buffer layer

thickening was observed in several studies where external forcing aimed at the reduction of wall shear stresses was employed [2, 5]. This effect is mainly attributed to the modification of the turbulent structures that gives rise to a readjustment of the energy budget between the turbulent kinetic energy production and the turbulence dissipation.

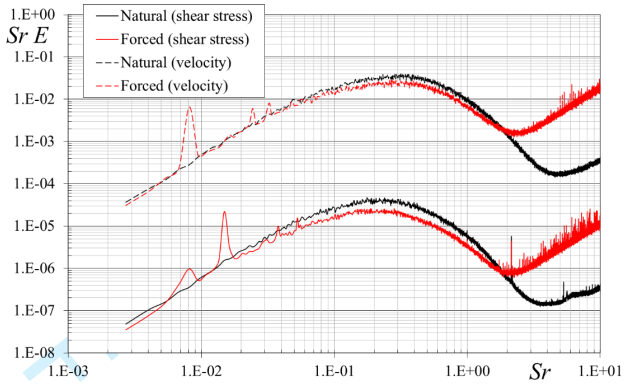

Fig. 14 Pre-multiplied velocity and wall shear stress spectra measured at y^+=12, Z/B=0.36 and X/H=38.

The velocity and wall shear stress pre-multiplied spectra measured at $y^+ = 12$, Z/B=0.36 and at $X/H = 38$ are reported in Fig. 14. Values are plotted against the non-dimensional frequency fH/U_c. Both velocity and wall shear stress energy spectra show the presence of peaks at low frequency in the forced configuration. We address these peaks to the forcing frequency. The wall shear stress spectra in the forced configuration feature lower energy values throughout a wide range of fH/U_c values, particularly in the inertial range. Even if the entity of such reduction is slightly smaller in the case of the velocity spectra, the overall behaviour is quite similar.

VI. Near wall structures modification

In this section the results related with the effects of the forcing on the near wall flow structure and events are presented.

A near wall turbulent flow is dominated by several coherent structures (low and high speed streaks, quasi streamwise vortices, legs of hairpin vortices, etc.) by shear layers differently oriented (sweeps and ejections) and others minor organized motions that give rise to a complex interaction that sustain the wall turbulence regeneration mechanisms. In particular Jeong et al. [40], Jimenez and Pinelli [41] and Blackwelder and Kaplan [42] pointed out that in the buffer region the dynamics of the streaky structures is strictly linked to the one of the streamwise vortices and play a key role for the sustainment of turbulence in wall bounded flows.

As reported by Schoppa and Hussain [8] the sinuous instability of the streaks directly affects the generation of new near-wall quasi-streamwise vortices feeding the regeneration of turbulence.

To underline this aspect, a statistical characterization of the near wall streaks was carried out. To identify the streaks, we followed the procedure presented by Schoppa and Hussain [8, 44] and by Iuso et al. [26]. Once identified, it is

possible to give an estimate of the number of streaks, their average spacing and their intensity. This last quantity was evaluated through the calculation of the maximum value of the derivative $\partial u'/\partial z$ at the streaks borders that can be assumed as the leading component of the wall normal vorticity fluctuation ω_y' and hence its strength. The analysis was performed in planes positioned at different wall distances in the range $7 < y^+ < 190$ and allows for a statistical description of the streaky structure in terms of number of streaks, their width, spacing and strength. The centre of the PIV field used for this investigation is located at X/H =0.38 and Z/B=0.36, with a streamwise and spanwise extent equal to $\Delta X^+ \approx 550$ and $\Delta X^+ \approx 640$, respectively.

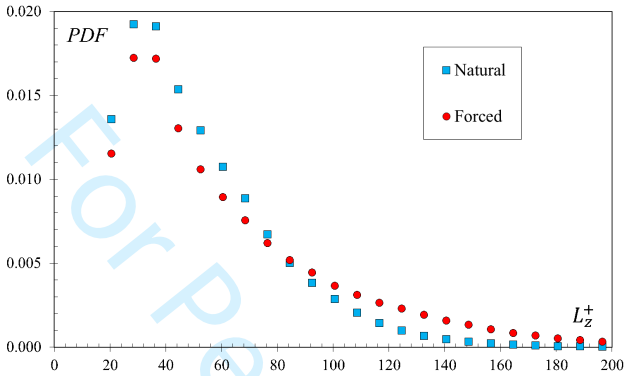

Fig. 15 PDF of the streaks' width for the natural and forced (L_{1-5} R_{6-10}, $f_f H/U_c$=0.0074) cases. Data are measured at y^+=12.

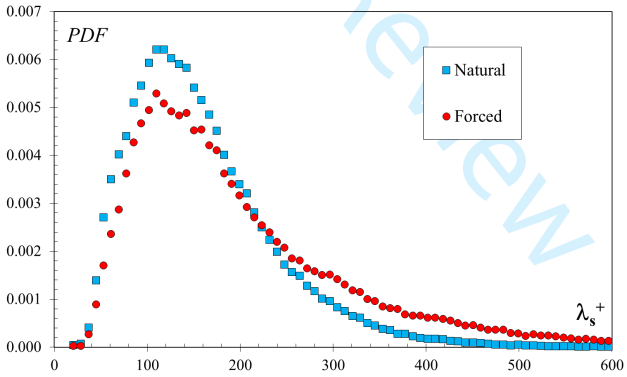

Fig. 16 PDF of the streaks' spacing for the natural and forced (L_{1-5} R_{6-10}, $f_f H/U_c$=0.0074) cases. Data are measured at y^+=12.

We find that the percentage variation of the educed streaks in the case of forced flow with respect to those of the natural flow is about 25%, at least for the investigated range of y^+. We address this reduction to the coalescence of the near wall structures and to their weakening that ultimately reduced the number of the most intense structures near the wall.

We further characterize the near wall structures by calculating the pdf of the width of the streaks and of their spacing, as reported in Fig. 15-Fig. 16. As it can be observed in Fig. 15, streaks having width lower than approximately $L_z^+ \approx 80$

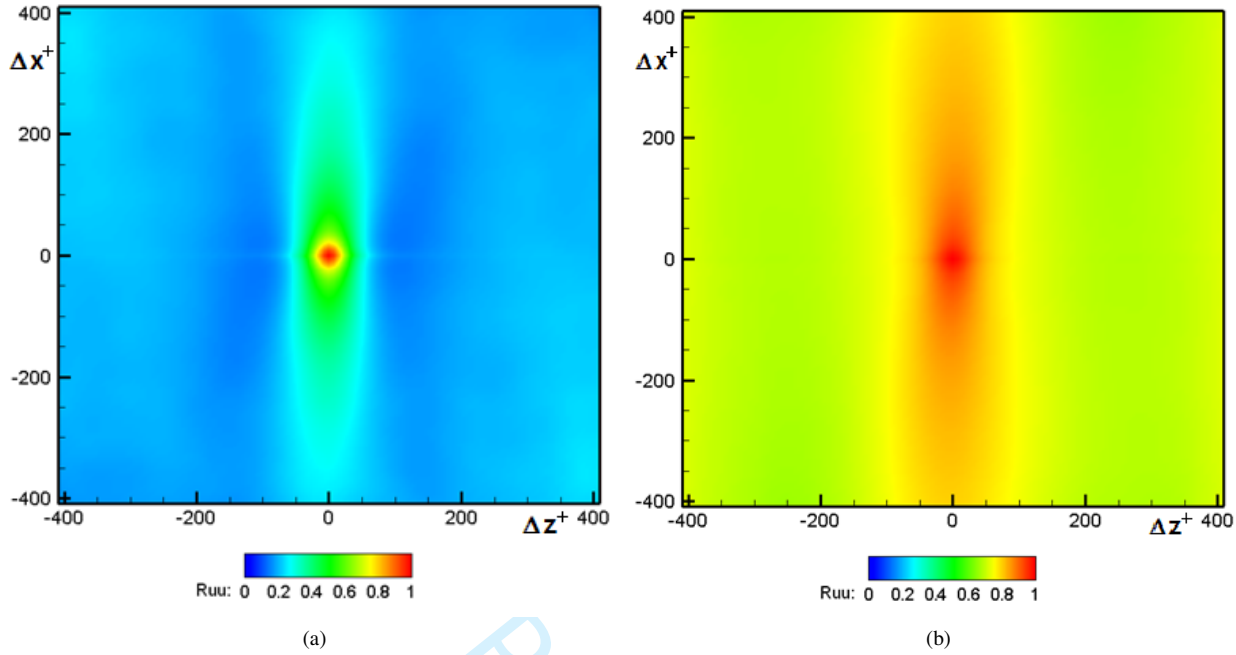

Fig. 17 Contour plot of the autocorrelation function $R_{u'u'}$ measured at y^+=12 for the natural flow (a) and the forced flow ($\mathbf{L}_{1-5}$ $\mathbf{R}_{6-10}$, $f_f H/U_c$=0.0074).

evidence a lower probability to be present in the manipulated flow. Instead, wider streaks (characterized by $L_z^+ > 80$) are more frequent when the forcing is present, thus reinforcing the conclusion of merging of the near wall structures due to the control mechanism.

In Fig. 16 the pdf of the streaks' spacing shows that the most probable value is around $\lambda^+ \approx 100$, which is the typical value for wall bounded turbulent flows. Consistently with the previous results, the forcing increases the probability to find higher values of the spacing between streaks.

Fig. 17 shows the autocorrelation function $R_{u'u'}$ for the natural (a) and the forced flow (b). The natural flow shows an elongated structure of the autocorrelation function, featuring a drastic drop in the spanwise direction and higher correlation values in the streamwise one. In particular, values of $R_{u'u'}>0.25$ are kept for nearly $\Delta x^+ \approx 800$, whereas in the spanwise direction $R_{u'u'}$ attains values close to zero within $\Delta z^+ \approx 100$. The extent of the correlation length in both directions is close to the typical size of the near wall streaks.

In the forced flow case, a significant increment of both streamwise and transversal size of the streaky structure appears evident from Fig. 17. In fact, large values of $R_{u'u'}$ both in the streamwise and in the spanwise direction suggests a growth in the average size of the coherent structures near the wall. We address this to the effect of the forcing mechanism, which promotes the coalescence of the streaks, consequently leading to their size growth.

Another effect of the forcing is the weakening of the streaks' strength. In Fig. 18 we report the PDF of $|\frac{du'}{dz}|^+_{max}$. This quantity accounts for a significant share of the wall normal vorticity fluctuation ω'_y. Fig. 18 evidences a significant

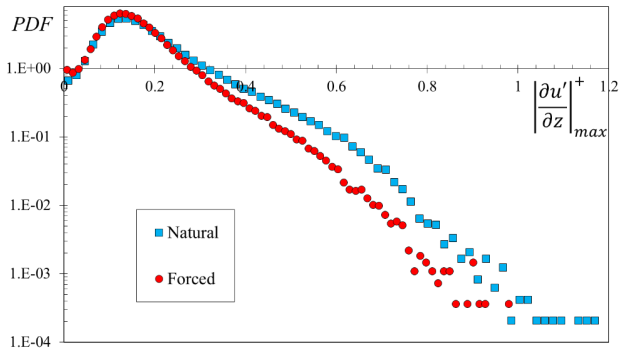

Fig. 18 PDF of $|\frac{du'}{dz}|^{+}_{max}$ for the natural flow (a) and the forced flow (L_{1-5} R_{6-10}, $f_f H/U_c$=0.0074) cases. Data are measured at $y^+ = 12$.

reduction of the streaks' strength in the case of forced flow, consistently with the previously discussed results. As also pointed out by Jimenez and Pinelli [41] and Schoppa and Hussain [8], ω'_y is a key indicator for the generation of quasi streamwise vortices, which are essential ingredients to sustain the wall turbulence regeneration mechanism.

It is interesting to notice that the PDF showed in Fig. 18 closely resembles the features of other forced flows characterized by different forcing mechanisms; for instance, for the case of a turbulent boundary layer manipulated with spanwise wall oscillation[7] or with steady couples of counter-rotating longitudinal vortices [10]. This common aspect can be reasonably associated to the common reaction of the forced flows in spite of the different forcing, due to common effects of weakening of the key structures (the low and high speed streaks) involved in the mechanism of the wall turbulence self-sustaining cycle, at least for the three considered flows.

VII. Scaling of the forcing

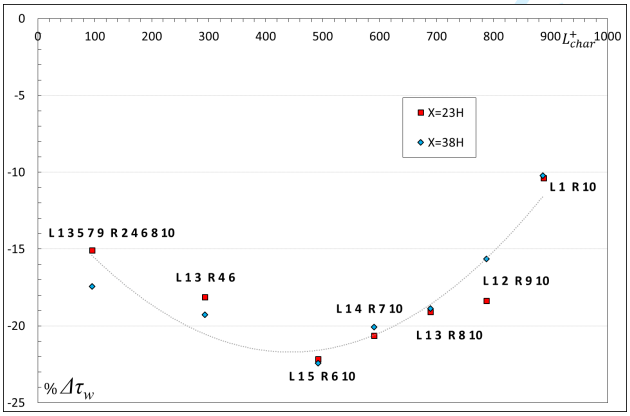

Fig. 19 Maximum drag reduction as a function of the dimensionless array characteristic length L^+_{char}. Forcing configuration $f_f H/U_c$=0.0074.

An attempt to find an appropriate scaling for the configuration of forcing jets was finally performed. Each injection

configuration can be characterized by a typical characteristic length (L_{char}) in the streamwise direction related to the distance between the centres of the two synthetic jet arrays connected with the two actuators. This length scale gives an idea of the streamwise length of influence of each control configuration.

In Fig 19, the maximum drag reduction (expressed as $\%\Delta\tau_{w,max} = 100 \cdot (\tau^f_{w,max} - \tau_{w,max})/\tau_{w,max}$, where the apex f indicates the forced flow condition) achieved for each tested configuration is shown as a function of L^+_{char}. The results refer to two streamwise positions, X/H=23 and X/H=38, and to the forcing frequency $f_f H/U_c$ =0.0074.

It can be observed that, for both streamwise distances the forcing configurations tested show a maximum of drag reduction for the array L_{1-5} R_{6-10} in correspondence of a value that is around L^+_{char} ≈500, which is nearly half of the typical length of the low speed streaks. It is then possible to infer that the optimal control mechanism must be characterized by a length of influence that can tamper at the most with the near wall dominant structures.

In this light, the forcing introduced by the configuration L_{1-5} R_{6-10} along with the forcing frequency ($f_f H/U_c$=0.0074) generates an oscillating large scale vortical structure that seems appropriately tuned on the typical length scale of the streaky structures at the Reynolds number of the experiment.

Conclusions

A fully developed turbulent channel flow forced by means of synthetic jets arrays was analysed experimentally, varying the array configurations and the forcing frequencies. The injection was operated tangentially to the upper horizontal wall and transversally to the main flow. For a specific array configuration (L_{1-5} R_{6-10}) and forcing frequency ($f_f H/U_c$=0.0074), detailed investigations in the spanwise and streamwise directions highlighted a strong persistence of the forcing effects in the streamwise direction, at distances as large as 150 channel half-heights. Moreover, integrated spanwise percentage variations of mean wall shear stress and of RMS value of skin friction fluctuations showed both channel walls to be in conditions of drag reduction and weakened near-wall turbulence.

In spite of the high turbulence level introduced in the main flow through the synthetic jets, it is possible to detect a global attenuation of the wall turbulence intensity in a large streamwise portion of the channel. The unsteady nature of the forcing associated with the streamwise modulation due to the array configuration, determined the generation of a large scale streamwise vortical structure that for the selected forcing parameters (array configuration and forcing frequency) was appropriate for the modification of the near wall structures, producing wall shear stress reduction and near wall turbulent fluctuations attenuation.

The results suggest that the forcing causes a partial suppression or at least attenuation of the near wall structures; in particular, they result to be weakened by the forcing mechanism and statistical results suggest their coalescence, as also showed by Yao et al. [11] in similar conditions.

The forcing gives rise to a large scale vortical structure that manipulates the flow by three mechanisms: the upflow, downflow and cross flow effects.

The upflow produces the lifting effect of the near wall structures (low speed streaks and quasi streamwise vortices) displaces the quasi streamwise vortices outward, thereby reducing the direct transport of high speed fluid towards the wall and determining the reduction of the wall shear stress.

In the downflow region, the wall-ward motion tends to flatten the near wall layers. As a consequence, the downflow prevents the near wall structures instability. Finally, the cross-flow regions originate beneficial effects through the coalescence of the near wall coherent structures.

Finally, by defining a length-scale which is related to the extent of the forced portion of the flow, an optimal forcing configuration can be identified. The results show that the highest effectiveness is obtained when, for a fixed value of the forcing frequency ($f_f H/U_c$=0.0074), the characteristic length-scale of the forcing normalised with respect to the wall quantities is about 500.

Acknowledgments

The authors are grateful to the technicians Marcello Marsili and Marco Grivet for their assistance during the experimental set up and to the students L. Caccamo, C. De Lumè and L. Acerno for their help during the experimental investigations.

References

[1] Jung, W. J., Mangiavacchi, N., and Akhavan, R., "Suppression of turbulence in wall-bounded flows by high-frequency spanwise oscillations," *Physics of Fluids A*, 1992. doi:10.1063/1.858381.

[2] Choi, K.-S., DeBisschop, J.-R., and Clayton, B. R., "Turbulent boundary-layer control by means of spanwise-wall oscillation," *AIAA Journal*, 2012. doi:10.2514/3.13948.

[3] Choi, K. S., "Near-wall structure of turbulent boundary layer with spanwise-wall oscillation," *Physics of Fluids*, 2002. doi:10.1063/1.1477922.

[4] Straub, S., Vinuesa, R., Schlatter, P., Frohnapfel, B., and Gatti, D., "Turbulent Duct Flow Controlled with Spanwise Wall Oscillations," *Flow, Turbulence and Combustion*, 2017. doi:10.1007/s10494-017-9846-6.

[5] Baron, A., and Quadrio, M., "Turbulent drag reduction by spanwise wall oscillations," *Applied Scientific Research*, 1995. doi:10.1007/BF00856638.

[6] Gatti, D., and Quadrio, M., "Reynolds-number dependence of turbulent skin-friction drag reduction induced by spanwise forcing," *Journal of Fluid Mechanics*, 2016. doi:10.1017/jfm.2016.485.

[7] Di Cicca, G. M., Iuso, G., Spazzini, P. G., and Onorato, M., "Particle image velocimetry investigation of a turbulent boundary layer manipulated by spanwise wall oscillations," *Journal of Fluid Mechanics*, 2002. doi:10.1017/S002211200200157X.

[8] Schoppa, W., and Hussain, F., "A large-scale control strategy for drag reduction in turbulent boundary layers," *Physics of Fluids*, 1998. doi:10.1063/1.869789.

[9] Iuso, G., Onorato, M., Spazzini, P. G., and Di Cicca, G. M., "Wall turbulence manipulation by large-scale streamwise vortices," *Journal of Fluid Mechanics*, 2002. doi:10.1017/S0022112002002574.

[10] Di Cicca, G. M., Iuso, G., Spazzini, P. G., and Onorato, M., "PIV study of the influence of large-scale streamwise vortices on a turbulent boundary layer," *Experiments in Fluids*, 2002. doi:10.1007/s00348-002-0510-z.

[11] Yao, J., Chen, X., Thomas, F., and Hussain, F., "Large-scale control strategy for drag reduction in turbulent channel flows," *Physical Review Fluids*, Vol. 2, No. 6, 2017, p. 062601. doi:10.1103/PhysRevFluids.2.062601.

[12] Yao, J., Chen, X., and Hussain, F., "Drag control in wall-bounded turbulent flows via spanwise opposed wall-jet forcing," *Journal of Fluid Mechanics*, 2018. doi:10.1017/jfm.2018.553.

[13] Canton, J., Örlü, R., Chin, C., and Schlatter, P., "Reynolds number dependence of large-scale friction control in turbulent channel flow," *Physical Review Fluids*, Vol. 1, No. 8, 2016, p. 081501. doi:10.1103/PhysRevFluids.1.081501.

[14] Canton, J., Örlü, R., Chin, C., Hutchins, N., Monty, J., and Schlatter, P., "On Large-Scale Friction Control in Turbulent Wall Flow in Low Reynolds Number Channels," *Flow, Turbulence and Combustion*, Vol. 97, No. 3, 2016, pp. 811–827. doi:10.1007/s10494-016-9723-8.

[15] Jukes, T., Choi, K.-S., Johnson, G., and Scott, S., "Turbulent Drag Reduction by Surface Plasma Through Spanwise Flow Oscillation," 2012. doi:10.2514/6.2006-3693.

[16] Du, Y., Symeonidis, V., and Karniadakis, G. E., "Drag reduction in wall-bounded turbulence via a transverse travelling wave," *Journal of Fluid Mechanics*, 2002. doi:10.1017/S0022112001007613.

[17] Karniadakis, G. E., and Choi, K.-S., "Mechanisms on transverse motions in turbulent wall flows," *Annu. Rev. Fluid Mech*, 2003. doi:10.1146/annurev.fluid.35.101101.161213.

[18] Smith, B. L., and Glezer, A., "The formation and evolution of synthetic jets," *Physics of Fluids*, 1998. doi:10.1063/1.869828.

[19] Glezer, A., and Amitay, M., "SYNTHETIC JETS," *Annual Review of Fluid Mechanics*, 2002. doi:10.1146/annurev.fluid.34.090501.094913.

[20] Di Cicca, G. M., and Iuso, G., "On the near field of an axisymmetric synthetic jet," *Fluid Dynamics Research*, 2007. doi:10.1016/j.fluiddyn.2007.03.002.

[21] Orazi, M., Lasagna, D., and Iuso, G., "Virtual Shaping on NACA 0015 by Means of a High Momentum Coefficient Synthetic Jet," *International Journal of Flow Control*, 2012. doi:10.1260/1756-8250.3.4.255.

[22] Cafiero, G., Castrillo, G., Greco, C. S., and Astarita, T., "On the effects of square-fractal turbulators on the flow field generated by a synthetic jet actuator," *Experimental Thermal and Fluid Science*, 2019. doi:10.1016/j.expthermflusci.2018.12.005.

[23] Smith, B. L., and Glezer, A., "Jet vectoring using synthetic jets," *Journal of Fluid Mechanics*, 2002. doi:10.1017/S0022112001007406.

[24] Park, S. H., Lee, I., and Sung, H. J., "Effect of local forcing on a turbulent boundary layer," *Experiments in Fluids*, 2001. doi:10.1007/s003480100305.

[25] Iuso, G., and Di Cicca, G. M., "Interaction of synthetic jets with a fully developed turbulent channel flow," *Journal of Turbulence*, 2007. doi:10.1080/14685240601110088.

[26] Iuso, G., Di Cicca, G. M., Onorato, M., Spazzini, P. G., and Malvano, R., "Velocity streak structure modifications induced by flow manipulation," *Physics of Fluids*, 2003. doi:10.1063/1.1597680.

[27] Peet, Y., Sagaut, P., and Charron, Y., "Turbulent Drag Reduction Using Sinusoidal Riblets With Triangular Cross-Section," 2012. doi:10.2514/6.2008-3745.

[28] Grüneberger, R., and Hage, W., "Drag characteristics of longitudinal and transverse riblets at low dimensionless spacings," *Experiments in Fluids*, 2011. doi:10.1007/s00348-010-0936-7.

[29] Nugroho, B., Hutchins, N., and Monty, J. P., "Large-scale spanwise periodicity in a turbulent boundary layer induced by highly ordered and directional surface roughness," *International Journal of Heat and Fluid Flow*, 2013. doi:10.1016/j.ijheatfluidflow.2013.04.003.

[30] Sasamori, M., Mamori, H., Iwamoto, K., and Murata, A., "Experimental study on drag-reduction effect due to sinusoidal riblets in turbulent channel flow," *Experiments in Fluids*, 2014. doi:10.1007/s00348-014-1828-z.

[31] Chen, H., Rao, F., Shang, X., Zhang, D., and Hagiwara, I., "Flow over bio-inspired 3D herringbone wall riblets," *Experiments in Fluids*, 2014. doi:10.1007/s00348-014-1698-4.

[32] Spazzini, P. G., Iuso, G., Onorato, M., and Zurlo, N., "Design, test and validation of a probe for time-resolved measurement of skin friction," *Measurement Science and Technology*, 1999. doi:10.1088/0957-0233/10/7/309.

[33] Tardu, F. S., and Pham, C. T., "Response of Wall Hot-Film Gages With Longitudinal Diffusion and Heat Conduction to the Substrate," *Journal of Heat Transfer*, 2005. doi:10.1115/1.1928907.

[34] Shah, D. A., and Antonia, R. A., "Scaling of the "bursting" period in turbulent boundary layer and duct flows," *Physics of Fluids A*, 1989. doi:10.1063/1.857450.

[35] Hutchins, N., Nickels, T. B., Marusic, I., and Chong, M. S., "Hot-wire spatial resolution issues in wall-bounded turbulence," *Journal of Fluid Mechanics*, Vol. 635, 2009, pp. 103–136. doi:10.1017/S0022112009007721.

[36] Wietrzak, A., and Lueptow, R. M., "Wall shear stress and velocity in a turbulent axisymmetric boundary layer," *Journal of Fluid Mechanics*, Vol. 259, 1994, pp. 191–218. doi:10.1017/S0022112094000091.

[37] Greco, C. S., Ianiro, A., Astarita, T., and Cardone, G., "On the near field of single and twin circular synthetic air jets," *International Journal of Heat and Fluid Flow*, 2013. doi:10.1016/j.ijheatfluidflow.2013.03.018.

[38] Berk, T., and Ganapathisubramani, B., "Effects of vortex-induced velocity on the development of a synthetic jet issuing into a turbulent boundary layer," *Journal of Fluid Mechanics*, 2019. doi:10.1017/jfm.2019.279.

[39] Scarano, F., Benocci, C., and Riethmuller, M. L., "Pattern recognition analysis of the turbulent flow past a backward facing step," *Physics of Fluids*, 1999. doi:10.1063/1.870240.

[40] Jeong, J., Hussain, F., Schoppa, W., and Kim, J., "Coherent structures near the wall in a turbulent channel flow," *Journal of Fluid Mechanics*, 1997. doi:10.1017/s0022112096003965.

[41] Jiménez, J., and Pinelli, A., "The autonomous cycle of near-wall turbulence," *Journal of Fluid Mechanics*, 1999. doi: 10.1017/S0022112099005066.

[42] Blackwelder, R. F., and Kaplan, R. E., "On the wall structure of the turbulent boundary layer," *Journal of Fluid Mechanics*, 1976. doi:10.1017/s0022112076003145.

[43] Orlandi, P., and Jiménez, J., "On the generation of turbulent wall friction," *Physics of Fluids*, 1994. doi:10.1063/1.868303.

[44] Schoppa, W., and Hussain, F., "Coherent structure generation in near-wall turbulence," *Journal of Fluid Mechanics*, 2002. doi:10.1017/S002211200100667X.